Journal of Applied Mechanics and Technical Physics, Vol. 49, No. 3, pp. 362–368, 2008

DYNAMICS OF ELECTROCONVECTIVE STRUCTURES IN A WEAKLY CONDUCTING LIQUID

V. A. Il'in and B. L. Smorodin

UDC 532.5

The finite-amplitude evolution of electroconvective structures in a weakly conducting liquid with an electroconductive charge formation mechanism is examined. The liquid is in the electrostatic field of a horizontally placed capacitor and is heated from below, and the electric charge time constant is much shorter than the characteristic hydrodynamic time. The interaction between the electroconductive convection and thermogravitational convection is considered. The evolution of the supercritical structures is investigated by direct numerical simulation using the finite-difference method. The bifurcations leading to the formation of stationary and wave liquid flows are analyzed. Nonlinear modes of stationary convection and traveling waves with different space–time patterns are identified and investigated.

Key words: *Electroconvection, weakly conducting liquid, electroconductive instability, nonlinear modes.*

Introduction. Electric field can have a substantial effect on the convective motion of weakly conducting liquids due to specific electroconductive instability [1, 2]. In studies of weakly conducting liquids placed in electric fields, it is of interest to investigate the possibility of controlling the behavior of these liquids and their effect on electric currents and heat transfer in high-voltage devices. In the present work, we examine the interaction of thermogravitational instability [3] and electroconductive instability — a type of electric instability related to the charge induction due to a difference between the electric conductivities of the liquid at the hot and cold electrodes [4]. In the case of electroconductive instability, electrostatic convection is known to arise due to the excited oscillations [5, 6]. Here the frequency of neutral oscillations of the liquid dielectric depends on the electrophysical properties of this dielectric. Low-mode analyses have been performed of nonlinear electroconvection modes in an alternating electric field of a horizontally placed capacitor in the case of a weakly conducting liquid [7] and an ideal liquid dielectric [8]. Those studies found different modes of regular and chaotic oscillations.

This paper gives results of direct simulation of the dynamics of nonlinear electroconvective structures resulting from monotonic or oscillatory instability of a weakly conducting liquid in an electric field.

1. Formulation of the Problem. We consider a plane horizontal layer of a viscous incompressible, weakly conducting liquid subjected to a vertical electrostatic field $\boldsymbol{E}$ and a gravity field $\boldsymbol{g}$. The x axis is directed along the lower boundary of the layer, and the z axis is normal to the layer boundaries. The position of the perfect heat- and current-conducting capacitor plates heated to different temperatures, $T(0) = \Theta$ and $T(h) = 0$, corresponds to the coordinates $z = 0$ and h (h is the layer thickness, T is the temperature reckoned from a certain intermediate temperature in the layer, and Θ is the characteristic temperature difference). The case $\Theta > 0$ corresponds to heating from below. The field potentials at the upper and lower boundaries are $\varphi(h) = 0$ and $\varphi(0) = U$, respectively.

The behavior of the weakly conducting liquid in the electric field will be examined using an electrohydrodynamic approximation [6]. With a small temperature difference across the layer, the nonuniform electric conductivity depends on the temperature linearly: $\sigma = \sigma_0(1 + \beta_\sigma T)$ ($\beta_\sigma > 0$ is the temperature coefficient of electric conductiv-

Perm' State University, Perm' 614990; ilin1@psu.ru; smorodin@psu.ru. Translated from Prikladnaya Mekhanika i Tekhnicheskaya Fizika, Vol. 49, No. 3, pp. 20–27, May–June, 2008. Original article submitted July 16, 2007.

ity). In this case, convection can arise from electroconductive instability, This results in accumulation of a space electric charge, which interacts with the external electric field and can set the liquid in motion (even in zero-gravity conditions).

Generally, the electric force acting on unit volume of a weakly conducting liquid is given by

$$\boldsymbol{f}_e = \rho_e \boldsymbol{E} - \frac{1}{2}\, E^2 \nabla\varepsilon + \frac{1}{2}\,\nabla\Big(\rho\,\frac{\partial\varepsilon}{\partial\rho}\,E^2\Big). \tag{1}$$

Liquid motion can be due only to the first component of the force [the first term in (1)], which is the Coulomb force dependent on the free space charge. The second (dielectrophoretic) component [the second term in (1)], related to the spatially nonuniform dielectric permittivity ε, is of no significance here. This approach is justified by the physical properties of the liquids used in experiments, whose electric conductivity depends on temperature much more strongly than their dielectric permittivity. The third component of the force [the third term in (1)] redefines the hydrostatic pressure. Next, we assume that the largest potential difference across the capacitor does not exceed the critical value U_* above which the effect due to injection on the liquid flow becomes significant [2]. We examine electroconvection in the Boussinesq approximation, assuming that this electroconvection results from spatial nonuniformities of the density ρ and nonuniform electric conductivity σ of the liquid. In the heat-conduction equation, we neglect viscous dissipation and Joule heating [6].

The problem is solved in dimensionless variables nondimensionalized as follows: the time t is normalized to the quantity $\rho_0 h^2/\eta$, the distance r to h, the velocity v to χ/h, the temperature T to Θ, the potential φ to U, the field strength E to U/h, the pressure p to $\eta\chi/h^2$, and the charge density ρ_e to $\varepsilon U/h^2$. Here, ρ_0 is the density of the liquid at rest, η is the dynamic viscosity, and χ is the thermal diffusivity.

The condition $\beta_\sigma \ll 1$ allows us to employ the zero-induction approximation. This approach ignores the electric field due to charge redistribution in the liquid with electroconvective flows because it is insignificant compared to the external electric field.

We write the system of electroconvection equations in dimensionless form

$$\begin{gathered}
\frac{\partial \boldsymbol{v}}{\partial t} + \frac{1}{\mathrm{Pr}}\,(\boldsymbol{v}\cdot\nabla)\boldsymbol{v} = -\nabla p + \Delta\boldsymbol{v} + \mathrm{R}_\sigma\,\rho_e\boldsymbol{\gamma} + \mathrm{R}\,T\boldsymbol{\gamma},\\[2ex]
\mathrm{Pr}\,\frac{\partial T}{\partial t} + (\boldsymbol{v}\cdot\nabla)T = \Delta T, \qquad \operatorname{div}\boldsymbol{v} = 0,\\[2ex]
\mathrm{Pr}_e\,\frac{\partial \rho_e}{\partial t} + \frac{\mathrm{Pr}_e}{\mathrm{Pr}}\,(\boldsymbol{v}\cdot\nabla)\rho_e + \rho_e + \frac{\partial T}{\partial z} = 0,
\end{gathered} \tag{2}$$

$$\mathrm{R} = \frac{\rho_0 g\beta\Theta h^3}{\eta\chi}, \qquad \mathrm{R}_\sigma = \frac{\beta_\sigma\Theta\varepsilon U^2}{\eta\chi}, \qquad \mathrm{Pr} = \frac{\eta}{\chi\rho_0}, \qquad \mathrm{Pr}_e = \frac{\varepsilon\eta}{h^2\rho_0\sigma_0},$$

where R and R_σ are the thermal and electric Rayleigh numbers, respectively, Pr and Pr_e are the thermal and electric Prandtl numbers, respectively, β is the thermal expansion coefficient of the liquid, and $\boldsymbol{\gamma}$ is the unit vector in the upward direction.

In the case of rigid, perfect heat- and current-conducting capacitor plates, the boundary conditions are

$$z = 0\colon \quad \boldsymbol{v} = 0, \quad T = 1, \quad \varphi = 1; \qquad z = 1\colon \quad \boldsymbol{v} = 0, \quad T = 0, \quad \varphi = 0. \tag{3}$$

We consider solutions periodic along the x-axis with a period $L = 2\pi/k$ and with the velocity, temperature, and charge density dependent on two coordinates, the vertical and horizontal ones (k is the critical perturbation wavenumber). In the plane (x, z) we introduce a stream function ψ and a velocity vortex Φ:

$$v_z = -\frac{\partial\psi}{\partial x}, \qquad v_x = \frac{\partial\psi}{\partial z}, \qquad \Phi = \Delta\psi.$$

Consider the instantaneous relaxation of electric charges ($\mathrm{Pr}_e = 0$), which is the case when the time constant is much shorter than the characteristic hydrodynamic time. In this case, the system of electrothermal convection equations (2) for weakly conducting liquids becomes

$$\frac{\partial \Phi}{\partial t} = \frac{1}{\mathrm{Pr}}\Big(\frac{\partial \psi}{\partial x}\frac{\partial \Phi}{\partial z} - \frac{\partial \psi}{\partial z}\frac{\partial \Phi}{\partial x}\Big) + \mathrm{R}_\sigma \frac{\partial \rho_e}{\partial x} + \mathrm{R}\frac{\partial T}{\partial x} + \Delta\Phi,$$
$$\frac{\partial T}{\partial t} = \frac{1}{\mathrm{Pr}}\Big(\frac{\partial \psi}{\partial x}\frac{\partial T}{\partial z} - \frac{\partial \psi}{\partial z}\frac{\partial T}{\partial x} + \Delta T\Big), \qquad \rho_e = -\frac{\partial T}{\partial z}. \tag{4}$$

Boundary conditions (3) expressed in terms of the stream function are

$$z = 0: \quad \psi = 0, \quad \psi' = 0, \quad T = 1; \qquad z = 1: \quad \psi = 0, \quad \psi' = 0, \quad T = 0. \tag{5}$$

In the case of solutions periodic along the horizontal axis x, all functions characterizing the nonlinear motion satisfy the conditions $f(x + L, z, t) = f(x, z, t)$ at the vertical boundaries. Problem (4), (5) was solved numerically by the fractional step method, and the Poisson equation was solved by the successive overrelaxation method. The conditions imposed on the velocity vortex were written using the Thomas formula [9].

In the initial state, vorticity values corresponding to the rotation of the liquid in opposite directions were set for the velocity vortex at two cell points, and equilibrium distributions were adopted for the stream function, temperature, and charge density. The parameter continuation method was used to construct solutions with a new set of parameters. For stationary modes, a solution was found by the relaxation method. To identify the waves traveling in the layer, we traced the evolution of the maximum stream function in the cell and the evolution of the stream function at a certain point inside the layer.

2. Stationary and Wave Electroconvection Modes. Figure 1 shows the critical electric Rayleigh number R_σ versus the thermal Rayleigh number R. The data for the monotonic mode were taken from [6], and the data for the oscillatory mode with $\mathrm{Pr} = 1$ were calculated by the Runge–Kutta method. With increasing Rayleigh number, the critical electric Rayleigh number R_σ for the oscillatory instability (1) decreases, whereas the critical number R_σ for the monotonic mode of instability (2) increases. The domain of instability lies between the curves and the coordinate axes. According to linear theory, in the case $\mathrm{R} = 2500$, the electric field suppresses the monotonic convection mode at $\mathrm{R}_\sigma = 1550.3$, resulting in an equilibrium state with a critical wavenumber $k = 2.48$ ($L_0 = 2.53$) in the liquid. As the electric field intensity (for $\mathrm{R}_\sigma = 3962.5$) increases, the liquid flow becomes unstable, and an oscillatory convection mode with a wavenumber $k = 4.08$ ($L_0 = 1.54$) and frequency $\nu = 6.39$ sets in.

The nonlinear electroconvective motions established in the horizontal layer were calculated for $\mathrm{Pr} = 1$ and $\mathrm{R} = 2500$ (the dashed curve in Fig. 1) for cells with sizes along the x axis $L_0 = 2\pi/k$ and $L = 2L_0$ (k is the wavenumber of the critical perturbations predicted by linear theory). In the calculations, a rectangular 41×21 mesh was used. In test calculations on a 81×41 mesh, integral characteristics were obtained which differ by more than 10% from those obtained on the 41×21 mesh, the flow structure remaining unchanged. For the monotonic mode, the cell size was set equal to $L_0 = 2.53$, and for the oscillatory mode, a cell with a length $L_0 = 1.54$ or $L = 2L_0 = 3.08$ was considered.

First, calculations were performed for various values of the electric Rayleigh number with initial conditions in the form of two vortices present in the cell. The calculations resulted in a stationary mode and a wave mode, in line with the predictions of linear theory. Then, the domains of existence of these modes in the parameter space were found. As a variable characterizing the convection modes we used the period-average value of the maximum stream function $\bar{\psi}_{\max}$.

Figure 2 shows curves of $\bar{\psi}_{\max}$ versus the electric Rayleigh number for the stationary and wave modes established in the liquid layer. In the absence of the electric field ($\mathrm{R}_\sigma = 0$), supercritical heating leads to steady thermogravitational convection in the layer, whose intensity decreases with increasing electric intensity [the maximum stream function decreases (the dashed curve in Fig. 2)]. The stream function vanishes at $\mathrm{R}_\sigma = 1560$, (this value was obtained by extrapolating the dependence $\bar{\psi}^2_{\max}$ to equilibrium values). In an interval $\mathrm{R}_\sigma > 1560$ the liquid is in equilibrium. This is indicative of a bifurcation of the steady flows with respect to the equilibrium position with decreasing electric field strength. The threshold value R_σ for the onset of the monotonic mode differs by 0.7% from the value $\mathrm{R}_\sigma = 1550.3$ predicted by linear theory.

In the cell L_0, a long-duration transient process is observed near the oscillatory-convection threshold, at $\mathrm{R}_\sigma = 3950$ (according to linear theory, at $\mathrm{R}_\sigma = 3962.5$). Here the stream-function oscillation frequency $\nu = 6.22$ at any fixed point of the convection cell differs by 2.7% from the value $\nu = 6.39$ predicted by linear theory. On completion of the transient process, a two-vortex motion with a different (lower) frequency is established. The steady-state oscillations (curves 1–4 in Fig. 2) were found to correspond to traveling waves. The spatial structure

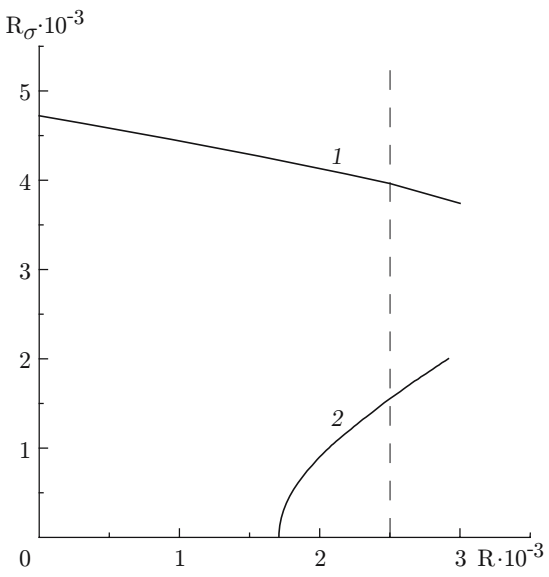

Fig. 1

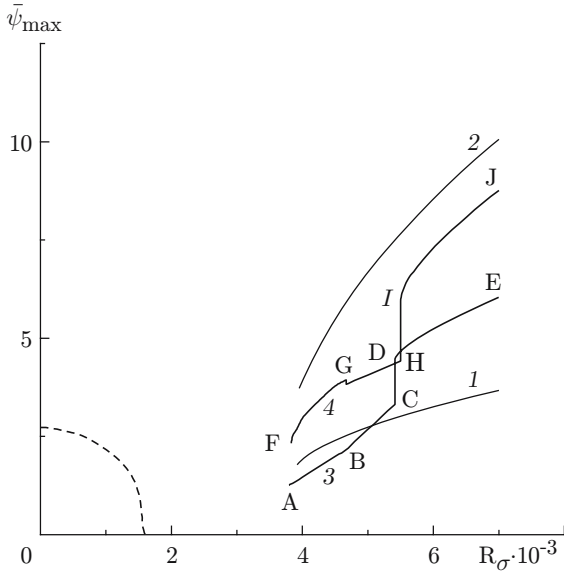

Fig. 2

Fig. 1. Domains of stability in the plane (R, R_σ) at Pr = 1: 1) boundary of the domain of oscillatory instability; 2) boundary of the domain of monotonic instability.

Fig. 2. Electroconvection modes at Pr = 1 and R = 2500: the dashed curve refers to the monotonic mode; curves 1 and 2 refer to $L_0 = 1.54$ for the wave traveling to the right and left, respectively; curves 3 and 4 refer to $L = 3.08$ for the wave traveling to the right and left, respectively.

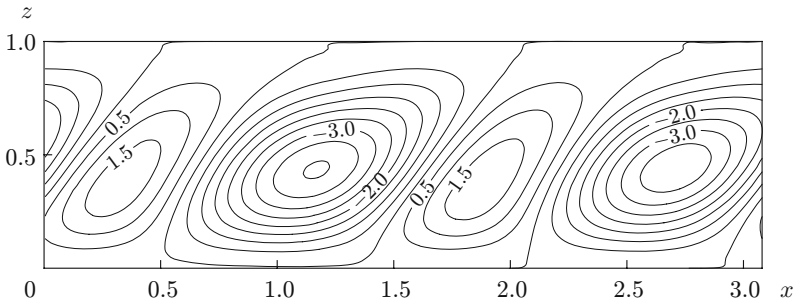

Fig. 3. Stream function field for the translationally symmetric mode (curve 1 in Fig. 2) at $R_\sigma = 4000$.

of the waves propagating in opposite directions (curves 1 and 2 or curves 3 and 4) is mirror symmetric with respect to the vertical plane and, hence, curves 2 and 4 in Fig. 2 also refer to the absolute value of the negative stream function for the wave traveling to the right (curves 1 and 3).

The waves corresponding to curves 1 and 2 in Fig. 2 are constant-amplitude waves. the mirror symmetry of each vortex with respect to the vertical plane is broken by the action of Coulomb forces. Furthermore, the intensities of neighboring vortices rotating clockwise and counterclockwise differ in value, which corresponds to translationally symmetric modes reproduced with a shift of these vortices for the length L_0 along the layer.

Figure 3 shows stream-function isolines for the mode corresponding to curve 1 in Fig. 2 at $R_\sigma = 4000$. With time, the isolines are shifted to the right. With increasing electric Rayleigh number, the intensity of the liquid motion increases: the stream function, dimensional heat transfer, and other integral characteristics increase. The vibration frequency reaches the value $\nu = 6.1$ at $R_\sigma = 7000$.

In the cell L, along with the translationally symmetric modes, modes were found that exhibit a more complex space–time behavior — asymmetric waves (curves 3 and 4 in Fig. 2).

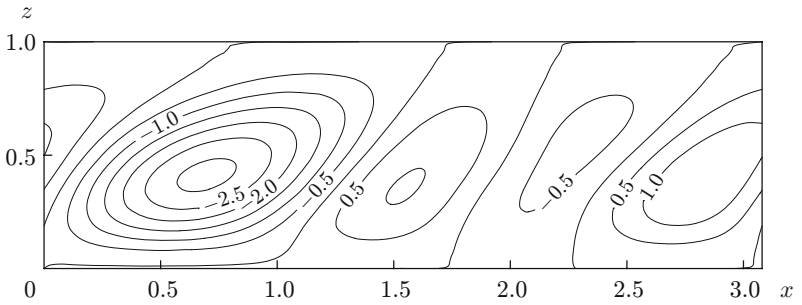

Fig. 4. Stream function field for the translationally asymmetric mode (curve 3 in Fig. 2) at $R_\sigma = 4000$.

As the electric Rayleigh number decreases, the first mode (curve 1 in Fig. 2) exists up to $R_\sigma = 3922$, at which the stream-function oscillation frequency at a fixed point of the cell is $\nu = 5.18$. At $R_\sigma < 3922$, after a long-duration transient process, the motion enters a mode that corresponds to curve 3 in Fig. 2. A distinctive feature of the asymmetric modes is that, on the cell length L, vortices are not reproduced twice. By way of example, Fig. 4 shows stream-function isolines for the third mode (curve 3 in Fig. 2) with $R_\sigma = 4000$. One can see two vortices differing in intensity and rotating clockwise and the two vortices rotating counterclockwise. A wave traveling to the right corresponds to this mode. Using the parameter continuation method, we found that the domain of existence of the third mode in the parameter space is bounded from below by the value $R_\sigma = 3796$, at which the period-average value of the maximum stream function equals $\bar{\psi}_{\max} = 1.26$.

At $R_\sigma < 3796$, the stream-function oscillations decay, the stream function vanishes, and an equilibrium state is established, which indicates a hard convection pattern (Hopf bifurcation). The threshold value of R_σ for the emergence of the oscillatory mode differs by 4% from the value $R_\sigma = 3962.5$ predicted by linear theory.

From the calculations, it follows that, with decreasing electric Rayleigh number, the mode corresponding to the wave traveling to the right (curve 2 in Fig. 2) exists up to $R_\sigma = 3954$, at which the oscillation frequency of the stream function equals $\nu = 5.21$. At $R_\sigma < 3954$, on completion of the transient process, the wave motion enters a fourth mode (curve 4 in Fig. 2). On the upper boundary of the examined interval ($R_\sigma = 7000$), the stream-function oscillation frequency corresponding to curve 2 in Fig. 2 is $\nu = 6.06$. Using the parameter continuation method, we found that the domain of existence of the fourth mode in the parameter space is bounded from below by the value $R_\sigma = 3830$. At $R_\sigma < 3830$, an equilibrium state sets in.

The slight difference between the values of R_σ for the waves traveling in opposite directions is likely due to the particular implementation of the numerical algorithm.

For the asymmetric modes, there are three types of motion exhibiting different space–time behaviors, depending on the value of the electric Rayleigh number R_σ,.

The first type of motion is an amplitude-modulated traveling wave (the segments AB and FG of curves 3 and 4 in Fig. 2). A distinctive feature of the mode is that, for the fixed electric Rayleigh number R_σ corresponding to the segments AB and FG, the total number of vortices and the field structure in the layer do not change with time. The vortices move to the right or to the left with their intensity being the only characteristic that undergoes changes — the vortices "are breathing." The change in the structure of the stream-function field for this type of motion is due to an increase of R_σ. As an example, we consider the evolution of the amplitude-modulated wave corresponding to curve 3 in Fig. 2. At $R_\sigma = 3796$, four vortices exist in the layer: two almost symmetric small positive vortices rotating counterclockwise and two large negative vortices rotating clockwise. At $R_\sigma = 3900$, one of the negative vortices begins to decrease in intensity, and at $R_\sigma = 4500$, the positive vortices adjacent to it merge together, resulting in three vortices remaining in the layer.

The second type of motion on the segments BC and GH (curves 3 and 4 in Fig. 2) exhibits a more complex space–time behavior: this is an amplitude-modulated traveling wave with the field structure changing with time (during the motion, the two-vortex becomes a four-vortex structure). Figure 5 shows the evolution of the stream function at a fixed point ($x = L/4$ and $z = 1/2$) and the minimum and maximum values of the stream function in the cell at $R_\sigma = 5000$.

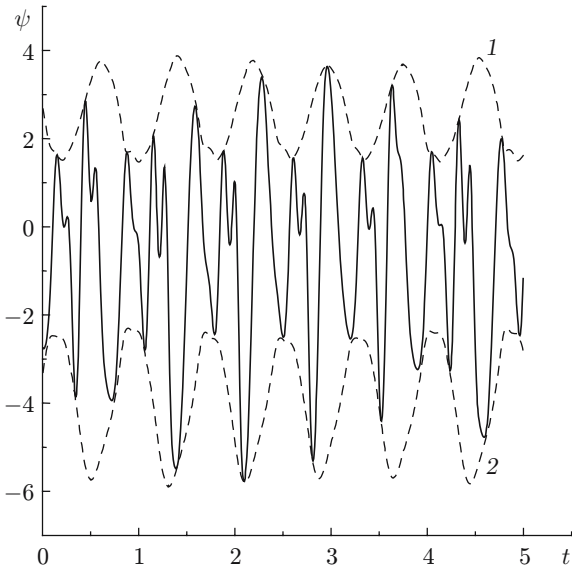

Fig. 5. Dependence $\psi(t)$ for $R_\sigma = 5000$: the solid curve is the amplitude-modulated traveling wave (the segment BC of curve 3 in Fig. 2); the dashed curves 1 and 2 show the maximal and minimal stream-function values, respectively.

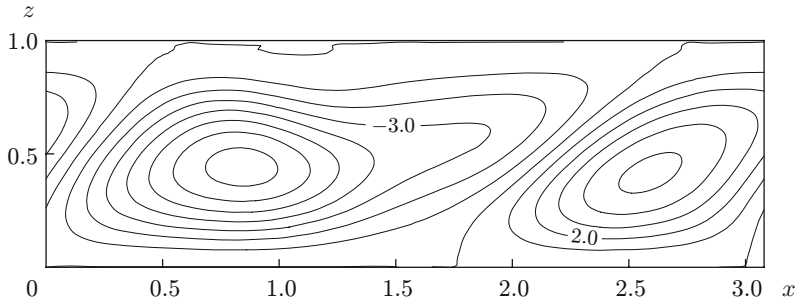

Fig. 6. Stream-function field for the third mode at $R_\sigma = 6000$ (the segment DE of curve 3 in Fig. 2).

On the segments DE and IJ of curves 3 and 4 in Fig. 2, the third type of wave motion occurs: a wave having a constant amplitude travels in the layer. The stream-function field is presented in Fig. 6. One can see two vortices: a positive vortex and a negative vortex extended along the x-axis; with time, the field structure remains unchanged and the vortices are shifted to the right. Between the segments BC and DE in Fig. 2, the transition occurs abruptly, and, in addition, a hysteresis transition was found: during motion from left to right in the parameter space, transition to the upper segment occurs at $R_\sigma = 5444$, and during motion in the opposite direction, transition from the upper to the lower segment occurs at $R_\sigma = 5414$.

Conclusions. The study was made of the nonlinear convective motion of a weakly conducting liquid with an electroconductive mechanism of instability in the electrostatic field of a horizontal capacitor heated from below.

The oscillations evolve into traveling waves in the layer. In the cell L_0, two traveling waves reproduced twice in the cell $L = 2L_0$ were identified (translationally symmetric modes). In addition, in the cell L, two asymmetric oscillatory modes exist. In addition to constant-amplitude traveling waves, amplitude-modulated traveling waves of constant or altered structure were identified.

This work was supported by the Russian Foundation for Basic Research (Grant Nos. 05-01-00789 and 07-01-96046).

REFERENCES

1. A. Castellanos, P. Atten, and M. G. Velarde, "Oscillatory and steady convection in dielectric liquid layers subjected to unipolar injection and temperature gradient," *Phys. Fluids*, **27**, No. 7, 1607–1615 (1984).
2. G. A. Ostroumov, *Interaction of Electric and Hydrodynamic Fields* [in Russian], Nauka, Moscow (1979).
3. G. Z. Gershuni, E. M. Zhukovitskii, and A. A. Nepomnyashchii, *Stability of Convective Flows* [in Russian], Nauka, Moscow (1989).
4. M. J. Gross and J. E. Porter, "Electrically induced convection in dielectric liquids," *Nature*, **212**, No. 5068, 1343–1345 (1966).
5. R. J. Turnbull, "Electroconvective instability with a stabilizing temperature gradient. 2. Experimental results," *Phys. Fluids*, **11**, No. 12, 2597–2603 (1968).
6. M. K. Bologa, F. P. Grosu, and I. A. Kozhukhar', *Electroconvection and Heat Transfer* [in Russian], Shtiintsa, Kishinev (1977).
7. V. A. Il'in and B. L. Smorodin, "Nonlinear electroconvection modes in a weakly conducting liquid," *Pis'ma Zh. Tekh. Fiz.*, **33**, Issue 8, 81–87 (2007).
8. V. A. Il'in and B. L. Smorodin, "Periodic and chaotic electroconvection modes in a liquid dielectric placed in a horizontal capacitor," *Pis'ma Zh. Tekh. Fiz.*, **31**, Issue 10, 57–63 (2005).
9. E. L. Tarunin, *Computing Experiment in Free-Convection Problems* [in Russian], Irkutsk State University, Irkutsk (1990).